Heat Transfer and Pressure Drop in Microchannels using sCO$_2$ for Solar Tower Applications

By

Muhammad Mohsin Tanveer

Reg# 00000119083

Session 2015-17

Supervised by

Dr. Muhammad Bilal Sajid

A Thesis Submitted to the US Pakistan Centre for Advanced study in Energy in partial fulfillment of the requirements for the degree of MASTERS of Science in

THERMAL ENERGY ENGINEERING

US-Pakistan Centre for Advanced Study in Energy (USPCAE)

National University of Sciences and Technology (NUST)

H-12, Islamabad 44000, Pakistan

Dec 2017

THESIS ACCEPTANCE CERTIFICATE

Certified that final copy of MS/MPhil thesis written by Mr. Muhammad Mohsin Tanveer (Registration No. 00000119083), of USPCAS-E (Institute) has been vetted by undersigned, found complete in all respects as per NUST Statues/Regulations, is free of plagiarism, errors, and mistakes and is accepted as partial fulfillment for award of MS/MPhil degree. It is further certified that necessary amendments as pointed out by GEC members of the scholar have also been incorporated in the said thesis.

Signature: _____

Name of Supervisor   Dr. Muhammd Bilal Sajid

Date: _____

Signature (HoD): _____

Date: _____

Signature (Dean/Principal): _____

Date: _____

Certificate

This is to certify that work in this thesis has been carried out by **Mr. Muhammad Mohsin Tanveer** and completed under my supervision in solar thermal laboratory, Centre for Energy Systems, National University of Sciences and Technology, H-12, Islamabad, Pakistan.

Supervisor: _____

Dr. Muhammad Bilal Sajid
USPCAS-E
NUST, Islamabad

GEC member # 1: **_____**

Dr. Adeel Javed
USPCAS-E
NUST, Islamabad

GEC member # 2: **_____**

Dr. Majid Ali
USPCAS-E
NUST, Islamabad

GEC member # 3: **_____**

Dr. Taqi Ahmad Cheema
FME
GIKI, sawabi

HoD-CES _____

Dr. Zuhair S Khan
USPCAS-E
NUST, Islamabad

Principal/ Dean **_____**

Dr. M. Bilal Khan
USPCAS-E

Dedication

I humbly dedicate this work to my parents whose endless prayers, continuous motivation and infinite sacrifices equipped me with everything it takes to be an accomplished human being.

Acknowledgment

I would like to thank my thesis advisor Dr. Muhammad Bilal Sajid of the USPCAS-E NUST. He is the driver of my research idea, from the formulation of the problem statement to the end result of my research. He consistently allowed this paper to be my own work, but steered me in the right direction whenever he thought I needed it. His directions were succinct and encouraging.

I would also like to express my profound gratitude to Dr. Adeel Javed and Dr. Majid Ali who helped me overcome the complications of ANSYS CFD. The door to their office was always open to me whenever I ran into a trouble regarding ANSYS. I also wish to thank Dr. Taqi Cheema who is an expert of micro-channels; his positive feedbacks steered my research.

I would also like to thank Dr. Brian Fronk of Oregon State University who is in charge of Thermal Energy Storage and Transport Lab. His expertise of the topic increased my overall understanding of the problem. Also, I am thankful to Dr. Kyle Zada who designed sCO_2 Experimental setup and helped me in my experimental work.

I am also thankful to my fellow lab members- Abdus Samad, Mehreen Fatima, Muhammad Akhter, Usman Salahuddin and Awais Mehboob for their continuous support and motivation.

Abstract

Energy is required to power the world. The demand for energy is rising rapidly. To fulfil this energy demand power plants are being engineered. Power plants are a major contributor to pollution. They emit carbon dioxide into the environment and causing global warming. To keep the environment safe, there is a need to move towards clean and renewable energy resources. There are many renewable resources available i.e. solar, wind, ocean wave, hydro and geothermal energy. All these resources have the potential for large-scale power production but their applicability depends upon the geographical location of the area and capital cost required. Among these resources, solar energy is in abundance in Pakistan. Solar energy can be harnessed using solar PV and solar thermal technology. Solar thermal technology is suitable for cogeneration and based upon conventional proven technologies. There are different methods to harness thermal energy from the sun but the solar tower has highest concentration ratio and can achieve a very high working fluid temperature. But there are complexities related to working fluid at such high operating conditions. Few of these are high operating pressure, fluid stability and corrosion and heat transfer properties. Supercritical CO_2 can be used in solar tower due to its favourable properties at such operating conditions. Micro-channels can be used to enhance heat transfer which improves thermal efficiency. In this research, a 3D rectangular microchannel is considered and heat transfer in near critical region is studied using ANSYS Fluent. Inlet mass flow rate, pressure and heat flux is varied to study their effects on heat transfer. Also, experiments are performed for pressure drop in microchannel test section and compared results with available pressure drop correlations. Due to sudden property variations, a peak in heat transfer coefficient is observed at the pseudocritical point. Also, it is found that available correlations are unable to predict accurately the pressure drop in microchannels for sCO_2.

Contents

List of Figures

List of Tables

List of Journals/Conference Papers

1. **Muhammad Mohsin Tanveer,** M.B Sajid "High flux solar thermal receiver using s-CO_2 in Microchannel" International workshop on sustainable energy development, November 2016, University of Agriculture Faisalabad

2. **Muhammad Mohsin Tanveer,** M.B Sajid **"**Effect of Micro-Channel Aspect Ratio on Pressure Drop and Heat Transfer" 7th International Conference: Environmentally Sustainable Aug 28, Abbottabad

3. **Muhammad Mohsin Tanveer,** M.B Sajid "Heat Transfer Study for Supercritical CO_2 in Microchannels" International Conference on Sustainable Energy Technologies, Sep 2017, Islamabad

4. **Muhammad Mohsin Tanveer,** M.B Sajid, Dr. Adeel Javed, Abdul Samad, Nouman Ali, Muhammad Usman "Heat transfer in microchannels using supercritical CO_2 for Solar Tower Applications" 2nd International conference on impact of Nanoscience on energy Technologies, 26 OCT 2017

5. Akhtar Abbas, Muhammad Bilal Sajid, **Muhammad Mohsin Tanveer**, " Concentrated Solar power generation feasibility in Pakistan" 2nd International conference on impact of Nanoscience on energy Technologies, 26 OCT 2017

6. Nouman Ali, Dr. Majid Ali, **Muhammad Mohsin Tanveer**, Abdulrab Asary, Hassan Nazir, Saba Aziz, Muhammad Amin Durrani "Designing of rectangular microchannel Heat exchanger based on thermal resistant network for waste heat recovery", " 2nd International conference on impact of Nanoscience on energy Technologies, 26 OCT 2017

List of Abbreviations

sCO$_2$	Supercritical CO$_2$
HTF	Heat transfer Fluid
T$_c$	Cold reservoir temperature
T$_h$	Hot reservoir temperature
Z	Compressibility factor
Nu	Nusselt number
h	Heat transfer coefficient
k	Heat conductance coefficient
D$_h$	Hydraulic Diameter
CFD	Computational fluid dynamics
T$_{in}$	Inlet temperature
T$_{out}$	Outlet temperature
T$_b$	Bulk fluid temperature
T$_w$	Wall temperature
A$_s$	Surface area in contact with fluid
w	Width of the channel
L	Length of the channel
H$_c$	Height of the channel
η_{fin}	Fin efficiency
A$_{seg}$	Segment area where heat flux is being applied
K$_{1-10}$	Minor loss coefficients
β	Diameter ratio at contractions or expansions
f$_t$	Friction factor
dP$_{channel}$	Pressure drop in channel
Re	Reynolds number
ε	Surface roughness
dP$_{minor}$	Minor pressure drop
DAQ	Data acquisition system
Pr	Prenatal number

1 Introduction

Energy is an utmost necessity for nations and. Sometimes prosperity of a country is correlated to per person energy consumption. But it comes at a very high cost. It has a major share in the annual budget and conventional energy sources have adverse effects on the environment. Nowadays, most of the energy is produced using fossil fuels which produce carbon dioxide (CO_2), a major source of global warming. About 90% of total CO_2 emission results from fossil fuel burning for power generation and transport sector [1]. Also, world's energy need is increasing rapidly and at the same time, fossil fuels are being depleted. To fulfil ever increasing energy demand and to protect the environment, the world should move towards renewable and clean energy resources.

There are different renewable energy options are available i.e. solar energy, Wind energy, geothermal energy and Wave energy. All of these energy resources can be utilized to fulfil world's energy need. Selection of suitable renewable energy source mainly depends on its resources and location. Pakistan has bright sunshine in most of its parts throughout the year. Its climate and geographical location are favourable for solar energy. So, solar energy is most suitable energy resource for Pakistan. At any moment, about 173000 terawatts of solar energy are striking the earth. It is 10,000 times more than world's energy use[2]. At Lahore, Solar radiation varies from 2.8 kWh/m^2/day-6.27 kWh/m^2/day[3].

1.1 Solar Thermal Technologies

Solar Energy can be harvested using different techniques. Two major techniques are Photovoltaic and solar thermal. In PV systems, solar energy is converted directly into electricity using semiconductor materials but PV cells have very low efficiency and higher manufacturing cost. In solar thermal technology solar energy is used to heat up some working fluid which is then used to produce steam. This steam is then used in conventional power cycle to produce electricity.

Solar thermal technology can be subdivided into 4 different systems based on their concentration ratio i.e. Flat plate collectors, solar parabolic trough, solar parabolic dish and solar tower. Concentration ratio is defined as the factor by which the incident radiation is enhanced on the receiver surface. It may also be defined as the ratio of the incident radiation on the receiver surface to radiation reaching earth surface.

In flat plate collector, Solar radiations are incident on a Coated metal sheets which absorbs thermal energy and transfer it to the heat transfer fluid (HTF) flowing in pipes attached to the absorbing plate. The absorbing plate is covered with a glass cover to reduce the convection losses. But still heat loss due to convection is quite high. To reduce this convective loss evacuated tubes are used in which there is a vacuum between the glass cover and absorbing plate.

To achieve high temperature concentrated technologies are used. They may be line focus or point focus. In line focus, radiations are concentrated on a line while in point focus, radiations are concentrated on a point. Point focus technologies have higher concentration ratio and can achieve higher temperatures. Parabolic troughs are line focus while concentrated dish and solar tower are examples of point focus technology.

Among all these technologies solar tower has highest concentration ratio and can achieve the highest temperature. The solar tower has the ability to be centralized for large power production as well as distributed power production.

1.2 Heat Transfer Fluids

Different fluids are used as HTF's in concentrated solar tower technologies. Few of them are Water, Air, Thermal oils and molten salts. Each of them has their own limitations and advantages. Thermal oils can operate at low temperatures and are good heat transfer properties but they have many hazards related to them. They are toxic to health, highly expensive and cause corrosion.

Molten salts have good heat transfer properties and have the ability to store energy but they freeze at a lower temperature. A secondary system is required to heat them up to their melting point. Their stability is also an issue at a higher temperature. They start degrading with the passage of time and cause corrosion in piping[4]. Gasses have very low heat transfer coefficient and power density. Water cause corrosion and have high pressure at higher temperatures.

CO_2 at supercritical state (sCO_2) is a good candidate for an HTF in the solar tower because of its favourable properties. If the temperature and pressure of a substance are above its critical point then it will be in the supercritical state. The critical point is a point on phase diagram at which liquid and gaseous phases have same density.

The pressure and temperature at critical point is known as critical pressure and critical temperature respectively. At supercritical state, fluid has intermediate properties of liquid and gaseous states. It has liquid-like density and gas like viscosity. sCO_2 has higher Brayton cycle efficiency. It obvious from Carnot cycle that higher temperature leads towards higher cycle efficiency.

$$\eta_c = 1 - \frac{T_c}{T_h} \qquad (1)$$

Where T_c and T_h are cold and hot reservoir temperature respectively. Rankine and Brayton cycles can be directly integrated with solar tower for large-scale power production and high temperature will improve cycle efficiency and reduce power production cost. Nowadays supercritical steam cycles are being utilized for higher efficiency. But there are material limitations for higher temperature. The higher temperature is associated with higher pressure and strong piping is required for safe operations. Critical pressure for steam is 22.064MPa. In heat exchangers, this thick piping due to high pressure leads towards lower thermal efficiency. Also, it increases the capital cost of the system. To solve these problems steam can be replaced by CO_2, which has favourable properties for heat transfer and have very low critical pressure i.e. 7.3 MPa, which is much lower than that of steam. Also, CO_2 has very low global warming potential as compared to the other refrigerants which make it useful as a refrigerant too. Another benefit of using sCO_2 is its compact turbomachinery and higher cycle efficiency.

1.3   Characteristics and benefits of s-CO$_2$
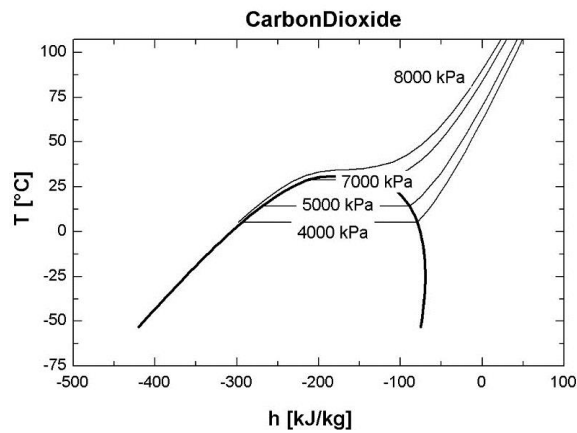
Figure 1 T-h diagram for CO$_2$

Figure 1 shows the T-h diagram for carbon dioxide for different operating pressures. With the increase in operating pressure, the boiling point is also increasing. It is also obvious from Figure 1 that with increasing pressure, vapour-liquid phase region is decreasing which ultimately vanishes at critical temperature and fluid directly converted to gas. Above this point, a substance exists in the supercritical state. Supercritical CO$_2$ has intermediate properties of gaseous and liquid phase. It has fluid-like density and gas like viscosity.

Material properties change rapidly in the near-critical region. The critical point for CO$_2$ is 31.1°C at 7.39MPa. Figure 2 shows density varies with temperature and pressure in near critical point. The density of CO$_2$ drops very rapidly in the near-critical region. This sudden variation of density decreases as we move away from the critical point.
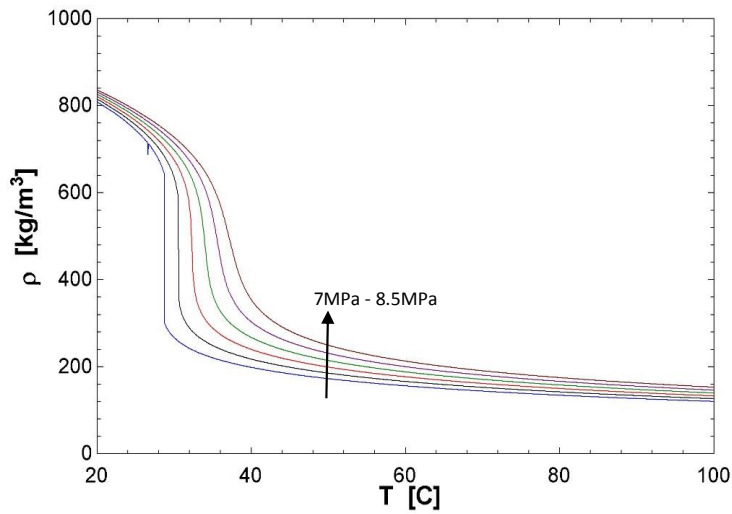
Figure 2 Effect of Temperature on density on near-critical region

Figure 3 shows the variation of specific heat with temperature. Specific heat touches a peak value at pseudo-critical temperature for a specific pressure value and remains smooth before and after pseudo-critical temperature. If the pressure is above the critical pressure then, the Pseudocritical temperature is a temperature at which heat capacity touches maximum value. Heat capacity is maximum at critical point and intensity of peaks decreases as we move away on either side of the critical point.

Figure 3 Effect of temperature on specific heat

Brayton cycle and Rankine cycle is used for power production from gas and steam respectively. Gases at normal pressures have a very high specific volume which results in low power density (i.e. power output per unit volume). At supercritical state, fluid has a very high density (low specific volume) as compared to gases. This leads to compact turbomachinery. This can be further explained by comparing Rankine and Brayton cycle efficiencies. Rankine cycle has higher efficiency as compared to Brayton cycle. The reason for this is that water is u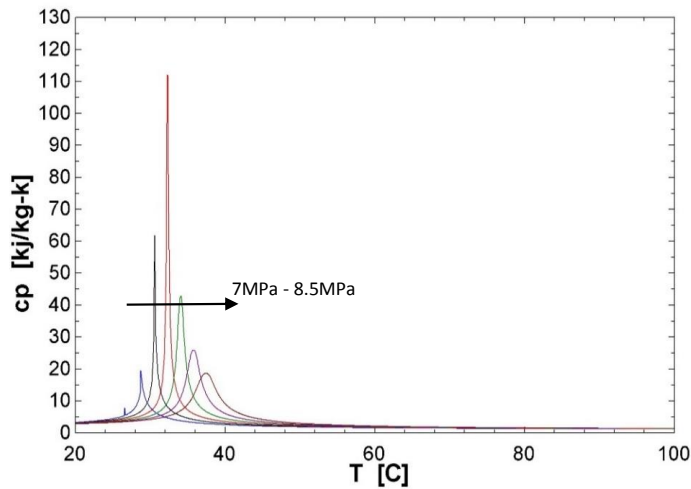sed in Rankine cycle which is incompressible and ideally, no work is required to compress the fluid. So, in the steam cycle, higher efficiency can be achieved at low inlet temperatures. While in Brayton cycle, air is used as working fluid. Air is compressible and a lot of energy is utilized to compress the air. So at higher inlet temperatures, Brayton cycle efficiency is not significantly higher than low-temperature steam cycle.

$$Z = \frac{P.M}{\rho.R.T} \tag{2}$$

The compressibility factor Z is defined as the molecular volumetric ratio of a fluid compared with ideal gas. It describes how close a fluid behaves relative to ideal gas. A value of one indicates fluid behaves very close to the ideal gas. CO_2 has very low compressibility factor in near critical region i.e. 0.2-0.5. That's why its power density is high and required turbomachinery size is small[5].

1.4 Microchannel

 The microchannel is a small confinement usually of hydraulic diameter less than a millimetre and is used for heat transfer enhancement. For constant surface temperature, the Nusselt number is constant (i.e. 3.657) for fully developed flows. The relation between Nusselt number and hydraulic diameter can be defined by using following equation. Heat transfer coefficient is inversely proportional to the hydraulic diameter and decreasing the hydraulic diameter will result in increased heat transfer coefficient.[6]

$$Nu = \frac{hD}{k} \tag{3}$$

$$h = 3.657\frac{k}{d} \tag{4}$$

They have wide applications in the electronics industry and are used for microprocessor cooling. They are used to cool high power processors. Specialized fluids are used to remove more heat while maintaining low temperatures. Also, the microchannel can be utilized in heat exchangers and solar tower to improve heat transfer which ultimately results in a reduction of heat exchanger size[7]. Currently, receiver size is large and major portion of the capital cost is used in the manufacturing of receiver. Receiver size can be reduced by using microchannel which will reduce overall capital cost and thermal efficiency.

2 Scope of Work

Solar tower size can be reduced using microchannel and efficiency of Brayton cycle can be greatly enhanced by using sCO_2. But steam cycles are used in power sector for a long time and very little knowledge is available related to sCO_2 as compared to steam cycles. So there is a great need to study sCO_2 to fully understand its flow dynamics and heat transfer characteristics. Most of the work which has been done already is related to large size channels (i.e. D_h >1mm). Due to large property variations, heat transfer coefficient can be enhanced or deteriorate by the effect of buoyancy or flow acceleration. How geometry shapes and dimensions affect this phenomenon is also not obvious. Also, experimental setup costs a lot and to develop test sections for microchannels and test them in a variety of conditions is very costly.

This research is focused to address these issues and develop a CFD model which predict heat transfer closer to the experimental results. This research can be subdivided into following major objectives.

1. Find out which turbulent model predict closer to the experiment results in microchannel
2. How heat transfer coefficient varies w.r.t temperature while keeping pressure constant and close to critical pressure
3. How mass flow rate and mass flux affects heat transfer microchannel
4. Effect of operating pressure on heat transfer
5. Effect of mass flow rate, operating pressure, inlet temperature on pressure drop

3 Literature review

Turbulent flows are normally utilized to improve heat transfer but it will also increase pressure drop. In turbulent flows, mixing of fluid produces near walls which contribute towards higher heat transfer coefficient. Different turbulent models are developed to predict turbulent flows. Modeling of turbulent flows with temperature dependent fluid properties is even more complex and convergence is slow.

The work on supercritical fluid heat transfer was first started in 1930. Schmidt et al. were working on developing new effective cooling systems for turbine blades in jet engines. They found that heat transfer coefficient is very high in near-critical region. The research in supercritical fluids proceeds with the aim to improve Brayton cycle efficiency. Also, critical fluids remain in single phase and complexities related to phase change can be avoided. In 1960, Different critical fluids were under consideration for different applications due to their properties. Conventional power plants were designed for supercritical conditions to be operated at higher efficiency. Several countries worked on supercritical water cooled reactors due to its enhanced heat transfer coefficient[8][9]. Supercritical CO_2 was considered as HTF due to its low critical pressure. Since then many types of research are carried out to fully understand its heat transfer behavior. This literature review will sum up different researches and their tested conditions for sCO_2.

Lio and Zhao[10] experimentally studied cooling heat transfer of supercritical CO_2 in mini and microchannels. Six different tube diameters are used. Operating parameters for the experiments were 74 to 1230 bar and flow rate of 0.02 to 0.2 kg/min. A temperature difference of an outer surface of tube length was negligible and also heat loss at both ends is kept the minimum. For same diameter tube and operating conditions, heat transfer coefficient reaches a maximum value near its pseudocritical point and then start decreasing. Also, the effect of tube diameter was studied and found that despite the high Reynolds number, there is still buoyancy effect exists and it becomes weaker as the tube diameter decreases.

Chen et al. [11] investigated heat transfer behaviour in the mini-channel for trans-critical CO_2. A CFD analysis of the circular tube at a pressure range of 7.4-8.0 MPa and flux of 10,000 to 90000 W/m2 was done and RNG k-e turbulent model was used for analysis. Multi peaks of heat transfer coefficient were obtained and these peaks

appeared at temperatures corresponding to the pseudocritical point at that pressure. Also, they suggested that buoyancy effect can be significant in mini-channels.

Chen et al. [12] also numerically studied near critical fluid mixing in a 2D transient microchannel of diameter 100 μm to 500 μm and found natural convection in these channels.

KOSHIZUKA [13] analyzed deterioration of heat transfer for supercritical water. He developed a 2D numerical model based on $k - \varepsilon$ mode and utilized steam table library for physical properties. He suggested that deterioration occurs mainly due to two mechanisms. As the flow rate increases, the viscosity of fluid also increases near the wall which increases the thickness of viscous sublayer and reduces Prandtl number. Also, heat flux value above the deterioration heat flux value causes wall temperature to oscillate.

Yoon [14] analyzed heat transfer and pressure drop characteristics in tube cooling of sCO_2 and compared the results with variously available correlations. sCO_2 was cooled by water in the tube in tube heat exchanger. Mass flux, an average pressure of test section and inlet temperature was varied to study how heat transfer coefficient and pressure drop changes. He found that peak value of heat transfer coefficient is achieved at the pseudocritical point and also it is higher at lower pressures. Also, for all cases, heat transfer coefficient increases with the increase of mass flow rate. Also, the measured pressure drop in the section was less than 1Kpa. Pressure drop increases at higher mass flux and also at lower system pressure. This can be explained by fact that density of fluid increases at higher pressures and turbulence of flow also increases at higher mass flux. The pressure drop was also compared with existing available pressure drop correlations and it was found that existing correlations underpredict the pressure drop.

Sharabi et al. [15] simulated deterioration of heat transfer in equilateral triangle shapes channel and square shaped channel. They concluded that RNG k-ε with two-layer treatment is unable to capture deterioration of heat transfer while all low Reynolds number models were able to capture the effect of buoyancy localized heat transfer deterioration.

Pandey [16]studied in tube cooling in a vertically oriented tube of diameter 2mm. the direct numerical simulation was done with operating pressure of 8MPa and it was

found that heat transfer is enhanced in flow in an upward direction due to the effect of deceleration and buoyancy while heat transfer is deteriorated in a downward direction.

Xiang [17] analyzed sCO_2 in horizontal tubes under cooling condition. A 2mm, 4mm, and 6mm diameter tubes were with varying input conditions. The length of the tube was 840mm which includes a fixed entrance length for boundary layer development. ANSYS CFX was used for analysis and SST k-w turbulent was used for turbulent flow modelling. Inlet Reynold number and inlet temperature and the outlet pressure are kept fixed. Numerical results were validated with experimental results and maximum and average error was found to be 13.5% and 3.8% respectively. It was found that wall temperature distribution was significantly nonuniform in circumferential direction due to buoyancy effect. Wall temperature was higher on the top surface as compared to the bottom surface. It was also found that heat transfer coefficient along the tube has a peak value at the pseudocritical point.

Liu et Al. [18] did experiments for sCO_2 heat transfer in large horizontal tubes and compare it with already developed correlations. Experiments were run for different operating conditions for three tube diameters of 4, 6 and 10.7. Inlet pressure for 1st two cases was kept constant (i.e. 8.0 MPa) while for 10.7 diameter tube operating pressure was varied from 7.5 MPa to 8.5MPa with an interval of 0.5MPa. It was found that peak heat transfer coefficient occurs at the pseudocritical point and shifted towards higher temperatures for higher operating pressures. Also, heat transfer coefficient increases with the increase of tube diameter. Heat transfer coefficient is also compared with already existing four correlations and the large deviation between measured and calculated data was found. Pressure drop decreases along the flow direction in cooling process ber5d7hcause of the decrease in density of the fluid. Decreasing density results in a reduction of average cross-section flow velocity.

Tanimizu and Sadr [19] experimentally investigate the effect of buoyancy on convective heat transfer coefficient. They used 8.7 mm circular tube and heat it using electric band heater on the outer surface. Copper block was used between test section tube and heater. The heated length of the tube was 1.14 m starting at 25mm

downstream of test section inlet. Thermocouples were installed at 65mm intervals to measure local wall temperature. The operating pressure and inlet temperatures ranges were 7.5-9.0Mpa and 20-28°C respectively. Wall heat flux and the mass flow rate were also varied. Wall temperature distribution shows a nonlinear behaviour. Heat transfer calculation shows enhancement and deterioration near the pseudo critical point. Results were also compared with normal heat transfer correlations and found that these correlations were unable to account for large property variations. Also, they over predict heat transfer coefficient even in regions away from the pseudocritical point.

Literature review shows that the most of the research is carried out for cooling on sCO_2 in large channels. No research is carried out for heat transfer behaviour and pressure drop in microchannels for sCO_2 in microchannels. This research is focused on to study how accurately simulations predict heat transfer coefficient in microchannels. Also, experiments are performed for pressure drop in microchannels.

4 Methodology

4.1 Simulation Methodology

4.1.1 Geometry

Simulations were performed for rectangular channels. It was similar to flow over rectangular fins. Channel design is similar to use by Kyle R. Zada for his experiments so that a comparison should be made[20]. It a square channel of 0.75mm. A half channel is modelled in ANSYS design modeller due to the symmetry of channel. Dimensions of the modelled channel is shown in Figure 5. Base heated depth is modelled in geometry to reduce computational power and it will be defined in boundary conditions in Fluent.
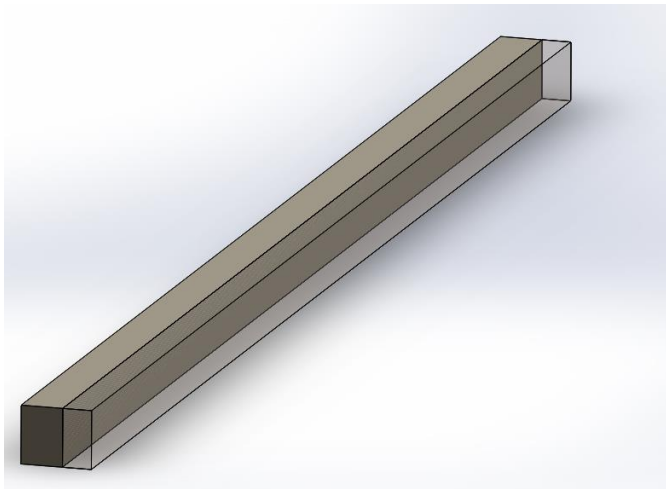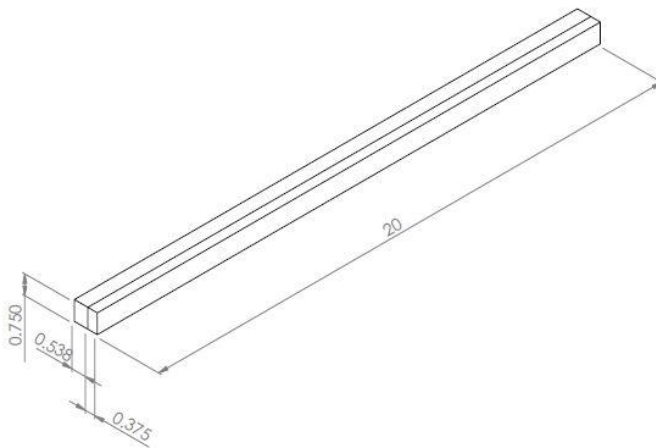

Figure 4 3D geometry of the channel

Figure 5 Dimensions of the channel modeled in ANSYS. All dimensions are in mm

4.1.2   Meshing

The meshing of the geometry is performed in ANSYS ICEM. ANSYS ICEM generates high-quality hexa mesh using blocking techniques. It has good features to control mesh parameters. Structured mesh is selected for simulations because less computational power is required for structured mesh and convergence is easy to achieve. Also, the geometry is simple so it is easy to make structured mesh.

The height of the channel has 60 nodes while the width of the channel is divided into 30 cells. There are 600 nodes along the length of the channel. The width of the fin has 20 nodes. A near wall node distance is 9e-7 to ensure y+ value less than 1. A cell growth ratio from the wall is 1.8.
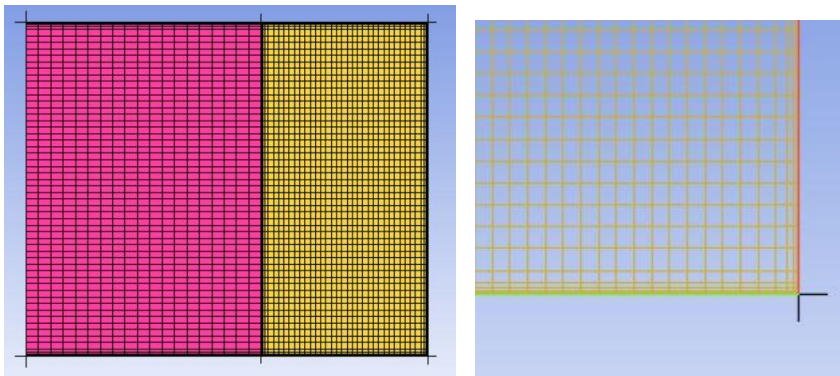
4.1.3   Solution methodology

The solution is performed in ANSYS Fluent 16.2. Available turbulent models were run for a specific case to find out which model predict closer to the experimental results. That model is used for further simulation cases. Gravity is turned on and gravitational acceleration of -9.81 is defined along the y-axis to capture the effect of buoyancy. At inlet mass flow boundary condition is defined. Heat flux is defined on the lower wall surface and wall width of 4mm is defined. Although modelling and meshing of this wall thickness will provide more accurate results that will increase computational power.

4.1.4   Simulation Matrix

A number of input parameters are varied to observe how these parameters affect the heat transfer in microchannels. Two different reduced pressures are selected for

simulations. For reduced pressure 1.1, 2 mass fluxes are simulated. For each mass flux and pressure case, the inlet temperature is varied from 25°C to 50°C with a higher resolution between 30°C to 40°C. All these test conditions are mentioned in the table below.

Table 1 Simulation Matrix

Case #	Reduced Pressure	Mass Flux (Kg/m^2-s)	Inlet Temperature ($^{\circ}$C)
1	1.1	5	25,30,32,34,35,36,38,40,50,100
2	1.1	10	25,30,32,34,35,36,38,40,50,100
4	1.03	10	25,30,32,34,35,36,38,40,50,100

4.1.5 Material Properties

National Institute of Standards and Technology (NIST) has a large material property database. This database contains fluid properties in pure form and also in mixture state. This material database is utilized for calculating temperature and pressure dependent properties of sCO2. NIST Reference fluid thermodynamic and transport properties database (REFPROF) is developed by NIST and is built in ANSYS Fluent for pressure and temperature dependent properties. It utilizes combined theoretical and predictive techniques based on evaluated data for fluid properties calculations. It covers a variety of fluids and their mixtures in different compositions.

For solid part of channel Haynes 320 steel is selected because, in available experimental results, this material was used. Following properties were found in the material data sheet and are defined in ANSYS Fluent.

Table 2 Haynes 320 steel properties, used for simulations

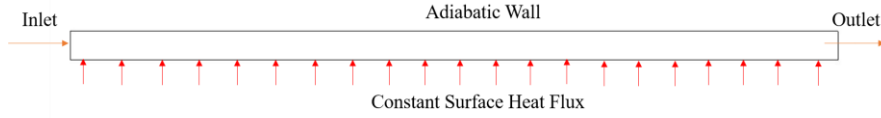| Property	Value
Density	8000 Kg/m^3
Specific heat	500 J/Kg-K
Thermal Conductivity	17.5 W/m-K

4.1.6 Boundary Condition

Figure 6 Boundary Conditions

Different boundary conditions which were used during simulations will be described in this section in detail. At inlet mass flow rate boundary condition is defined instead of velocity boundary condition because physical properties of sCO2 vary significantly with temperature. So for different inlet temperatures, the velocity of fluid will be different at the inlet. We have to keep the Reynolds number constant to observe how mass flow rate affects heat transfer. As fluid properties are being provided by NIST database so by using mass flow boundary condition system automatically calculate the velocity at the inlet. At the inlet, operating pressure and fluid temperature are also defined. Mass flow rate is calculated from mass flux using following formulas.

$$A_{c,t} = H.W \tag{5}$$

As we created symmetry for the channel so cross-sectional area will be half.

$$A_c = H.{W}/{2} \tag{6}$$

The mass flux defined in test matrix is for 5 channels. Mass flux in single channel will be one-fifth of total mass flux

$$G_{ch} = G/N_{ch} \tag{7}$$

$$\dot{m} = G_{ch}.A_c \tag{8}$$

$$Re = \frac{G_{ch}.d_h}{\mu_{sCO_2,i}} \tag{9}$$

The outlet of the channel is defined as the pressure outlet and operating pressure is defined here. Heat flux is defined on the bottom surface and symmetry boundary condition is defined along the right side of the channel.

4.2 Average Heat Transfer Coefficient Calculation

To calculate heat transfer coefficient, a similar methodology is used as adopted in the experimental setup by Kyle R. Zada [20]. Bulk temperature is calculated by taking an average of inlet and outlet temperature. Outlet temperature and wall temperature in Fluent is taken as area weighted average at outlet plane and plane created at bottom solid-liquid interface respectively.

$$T_b = \frac{T_{in} + T_{out}}{2} \tag{10}$$

Heat transfer coefficient is calculated using following formula

$$Q = h.A_s.(LMTD) \tag{11}$$

$$LMTD = \frac{(T_w - T_{in}) - (T_w - T_{out})}{ln\frac{(T_w - T_{in})}{(T_w - T_{out})}} \tag{12}$$

$$A_s = \left(\frac{w}{2} \times L\right) + (\eta_{fin}.H_c.L) \tag{13}$$

$$\eta_{fin} = \frac{tanh\left[\sqrt{\frac{2.\alpha_{sco2}}{k_w.t_{web}/2}}.(h_{chan} + \frac{t_{web}}{4})\right]}{\sqrt{\frac{2.\alpha_{sco2}}{k_w.t_{web}/2}}.(h_{chan} + \frac{t_{web}}{4})} \tag{14}$$

Total surface area subjected to heat flux is calculated as given below

$$A_{seg} = \left(\frac{w}{2} \times L\right) + (\frac{t_{web}}{2}.L) \tag{15}$$

4.2.1 Results Validation

To check the accuracy of the results, simulation results are validated with experimental results from OSU. In OSU an MS student Kyle R. Zada completed experiments for heat transfer in microchannels and similar geometry design is selected for simulation. Following are the different methods to ensure best simulation results.

- y^+ value is kept sufficiently below 1 to ensure simulation captures properly near wall effect.
- Increased the mesh size till variation in outlet temperature is negligible. This is done to reduce the effect of mesh size on simulation results.
- Finally, Simulation results are compared with experimental results and it is found that K-e realizable with standard wall function shows the best agreement with the experimental result.

4.3 Experimental Methodology

The pressure drop measured across the test section using differential pressure transducer is a sum of major and minor losses of the system. Major losses are the pressure drop that occurs inside channels while minor losses are the losses due to joints, fittings, bends, contraction, and expansion in pipes[21].

4.3.1 Minor Losses

Due to experimental limitations, it was not possible to measure pressure drop only across the microchannels so pressure drop across whole test section was measured and then minor losses are calculated analytically. The pressure drop due to minor losses is calculated as [22]:

$$dP_{minor} = K_L \rho \frac{v^2}{2} \tag{16}$$

4.3.2 Resistance Coefficient

Figure 7 shows a schematic diagram of the fluid path inside the test section. The test section is attached to the external loop using quarter inch pipe. This pipe is connected to the test section using the tapered threaded joint. Fluid from pipe then passes through a 90° bend which opens in channel inlet manifold. From inlet manifold, flow is distributed into 5 parallel channels. There are total ten minor losses

Comment [G1]: Inserted: ,

between differential pressure transducer which are explained in Table 3. Resistance coefficients were calculated for all these losses which are explained below.
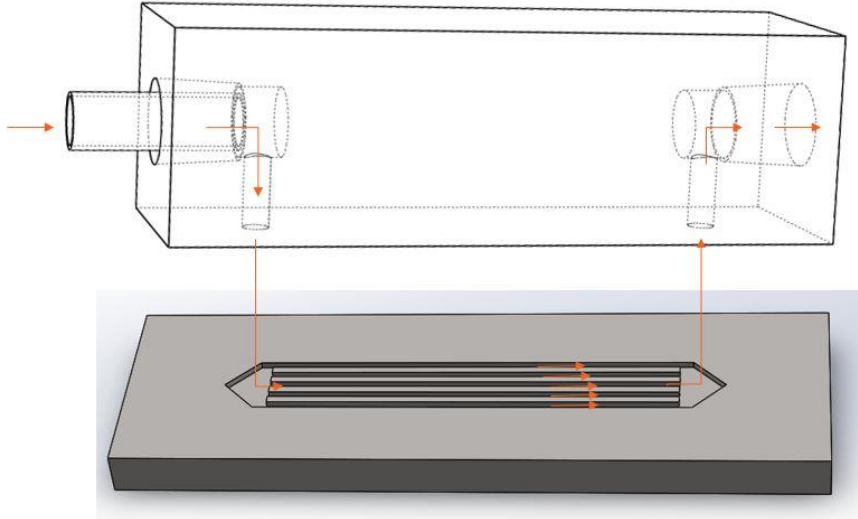

Figure 7 Schematic diagram for test section showing fluid path

Table 3 minor loss resistance coefficients

Resistance	Detail
K_{inlet} = Inlet side losses	
k_1	Sudden expansion
k_2	Sudden contraction
k_3	90^0 bend
k_4	Sudden contraction to inlet manifold
k_5	Sudden contraction to microchannels
K_{outlet} = Outlet side losses	
K_6	Expansion from microchannels to manifold
K_7	Expansion from Manifold
K_8	Sudden Expansion
K_9	90° bend
K_{10}	Sudden contraction

Contraction resistance coefficient can be calculated by using below given formula which shows that it depends on diameter ratio at the point of junction. [22]:

$$k = 0.5(1 - \beta^2)^2 \tag{17}$$

Where

$$\beta = \frac{d_1}{d_2} \tag{18}$$

Following formula can be found in the literature for expansion resistance coefficient. [22]

$$k = (1 - \beta^2)^2 \tag{19}$$

Change in direction of flow also causes pressure drops. When flow direction changes, separation may occur which causes sufficient amount of pressure drop. [22]. Bend friction factor can be calculated using following formula.

$$f_t = \frac{0.25}{\log\left[\frac{\varepsilon/D_{avg}}{3.7}\right]^2} \tag{20}$$

$$k = 30 \times f_t \tag{21}$$

So, total resistance coefficient will be

$$K_L = K_{total} = K_{inlet} + K_{outlet} \tag{22}$$

4.3.3   Friction Factor Correlations

The major loss is the pressure loss which occurs in the channels and our main focus is on this pressure drop. sCO_2 do not undergo a phase change in channels and it is

treated as single phase flows. Different correlations are available for pressure drop calculation for single phase flows which are described below.

The pressure drop inside the tube for turbulent flow can be calculated as [23];

$$dP_{channel} = f \frac{v^2 L}{2\rho D_i} \tag{23}$$

In above formula, all the parameters are flow conditions and there is a friction factor constant which depends on geometry and roughness of the material. Different correlations are experimentally developed to calculate the value of friction factor. One of the best correlation is Blasius correlation which was developed for turbulent flow in smooth tubes[24] and is given below;

$$f = 0.316 Re^{-1/4} \; for \; Re \; \leq 2 \times 10^4 \tag{24}$$
$$f = 0.316 Re^{-1/5} \; for \; Re \; \geq 2 \times 10^4$$

This Blasius equation is used for mini channels of 7.73mm diameter.

Among selected friction factor correlations, the next in line is Colebrook and white correlation and was used for friction factor calculation in 0.789mm diameter of the microchannel. This correlation is suitable for both turbulent and non-turbulent flow. [25].

$$\frac{1}{\sqrt{f}} = -2.\log\left[\frac{2.51}{Re.\sqrt{f}} + \frac{\varepsilon/d}{3.71}\right] \tag{25}$$

Xiande et al [26] used the Fang et al correlation for isothermal single phase conditions. The fluid used was R-22 and Reynold number range was 3000–10800.

$$f = 0.25\left[log\left(\frac{150.39}{Re^{0.98865}} - \frac{152.66}{Re}\right)\right]^{-2} \tag{26}$$

According to Lixin Cheng et al [27], Churchill correlation is vastly used friction correlation and is suitable for all flow regimes and relative roughness. Following equation represent the Churchill correlations:

$$f = 8 \left\{ \left(\frac{8}{Re_b}\right)^{12} + \frac{1}{\left[2.457 ln\left(\frac{1}{\left(7/Re_b\right)^{0.9} + 0.27\varepsilon/D}\right)^{16} + \left(\frac{37530}{Re_b}\right)^{16}\right]^{1.5}} \right\}^{1/12} \quad (27)$$

4.3.4 Total Pressure Drop

Finally, minor pressure losses and pressure drop in channel add up in the form of total pressure drop across the test section. This is the pressure drop, which differential pressure transducer will measure.

$$dp_{total} = dp_{minor} + dp_{channel} \quad (28)$$

4.3.5 Test Setup

Figure 8 shows a schematic diagram of the experimental test setup. After filling the system with CO_2 and pressurizing the system up to the required pressure, primary test loop consists of a pump, flow meter, test section and double pipe heat exchanger. Test loop starts with a pump which is a gear type pump and circulates the CO_2 inside the primary loop. Ahead of the pump, a pressure relief valve is connected to the loop which is used to manually reduce the pressure if the pressure inside the system is higher than the desired value. An automatic pressure relief valve is also present in the loop which will be automatically activated if the pressure inside the system is higher than the design pressure, to save the system from damage. After relief valve, a pressure transducer and Coriolis flow meter are present in the loop. If we go further downstream, test section is present whose schematics are shown in Figure 7. At the inlet of test section, a thermocouple and pressure transducer is attached to measure inlet temperature and pressure. CO_2 which exits the test section then enters into double pipe heat exchanger where ethylene glycol is flowing in secondary loop and

cool the CO_2. This is designed in a way to make sure that all the CO_2 that enters into the pump should be in the liquid state. A chiller is attached to the secondary loop to circulate cool ethylene glycol. All the thermocouples and pressure transducers are attached to a DAQ system which is then connected to the computer.
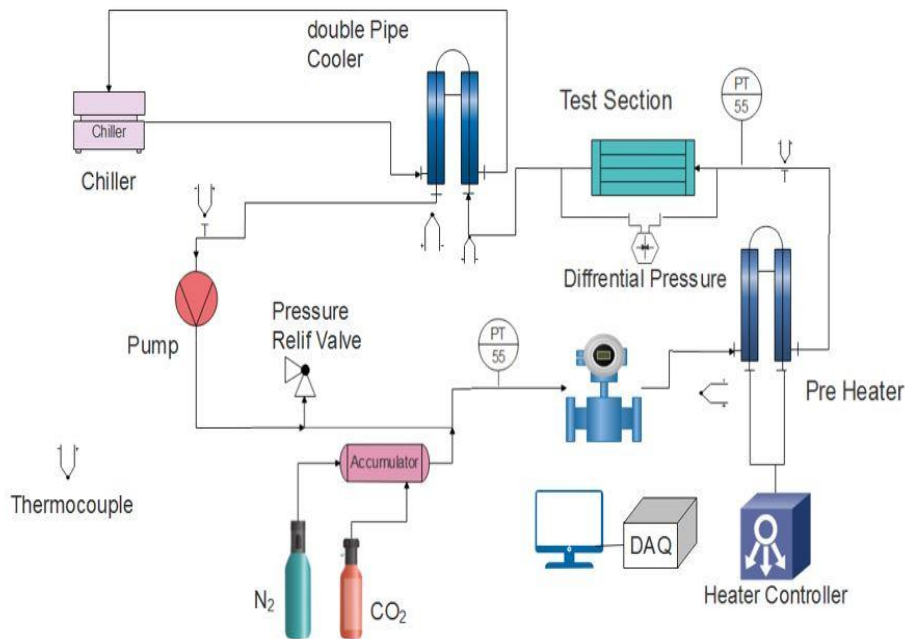

Figure 8 Schematic diagram of experimental setup

4.3.6   Operating Procedure

1st step in operation of the system is the charging of primary loop with CO_2. A vacuum pump is used to create a vacuum in the primary loop and then CO_2 Cylinder is attached to the accumulator to fill the system with CO_2. Once the system is charged with CO_2 it can be used for many experiments.

At the start of running an experiment, CO_2 is pressurized using a pressurized nitrogen cylinder. Once the system is pressurized up to desired value chiller is turned on and then pump is turned on to start the flow of CO_2 in the primary loop. 1st let the CO_2 to cool up to below 20°C and then its temperature is increased using preheater which is controlled by heater controller. Its temperature is increased gradually with an interval of 5°C. The pressure of the system is observed at each point and regulated

using relief valve and nitrogen cylinder. Once the system is reached up to the desired condition, it is observed for five minutes to ensure the steady state. After that data is recorded for 20 minutes.

4.3.7   Test Matrix

To perform the test two different reduced pressures were selected (i.e. 1.1 and 1.03). For reduced pressure 1.1 three different mass flow rates were chosen to observe the effect of Reynolds number on pressure drop. For a set of conditions inlet temperature was varied from 20°C – 50°C with a higher resolution between 30°C – 40°C.

Table 4Experimental Matrix

Section Number	Reduced Pressure	Mass Flow Rate (Kg/hr)	Inlet Temperature ($^\circ$C)
1	1.1	5	20-50
2	1.1	10	20-50
3	1.1	20	20-50
4	1.03	10	20-50

5 Results and Discussion

5.1 Heat Transfer

Heat transfer is greatly affected by buoyancy and flow acceleration. Flow acceleration is caused by density variation. As, the density of the fluid decreases while heating the fluid, the velocity of the fluid increases to conserve mass flow. Also, Buoyancy causes hotter fluid to rise up inside channel which may result in secondary flows. But it mostly depends on the ratio of Grashoph number to Reynolds number. If the ratio is very less than 1 than forced convection is dominant.

Figure 9, Figure 10, Figure 11 and Figure 12 shows velocity contours along the y-z axis at 34°C for various inlet conditions. It is observed that for low mass flow rate and heat flux, there exist some secondary flows.   For all other cases, forced convection is dominant and no secondary flow vectors are observed. The main reason for this is that Reynolds number for all test conditions is very high and flow is highly turbulent which suppresses secondary flows.
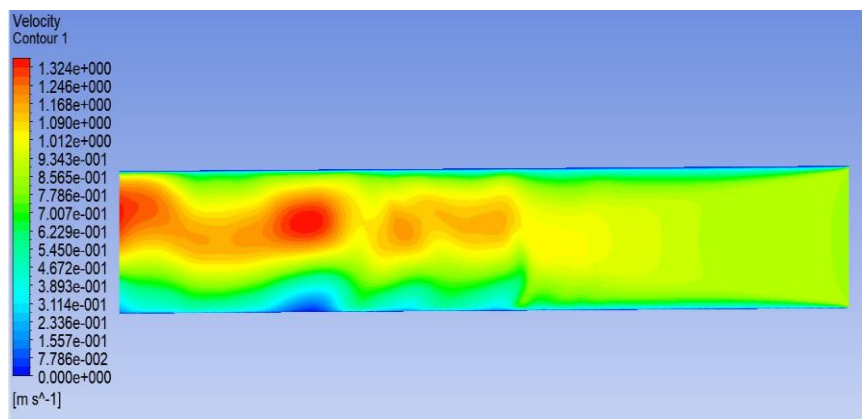

Figure 9 velocity distribution along a y-z plane at P=8170Kpa, m=500kg/hr.m², T_{in}=307

Another effect which is observable from velocity contours is boundary layer development. For the non-heated channel, there exists a symmetry along the centerline of the channel. But for the heated channel, no such symmetry exists. The slope of the boundary layer higher near the heated surface of the channel. This shows that velocity of the fluid is higher at top of the channel as compared to the bottom, although wall is present on both sides of the flow. The only difference is that bottom wall is heated. High-temperature fluid rise to the top due to its low density and heavy fluids comes to the bottom.

Also, even after the development of the boundary layer, the velocity of the fluid is increasing. This is caused by flow acceleration. The density of fluid decreases with heating results in an increase of velocity along the channel.
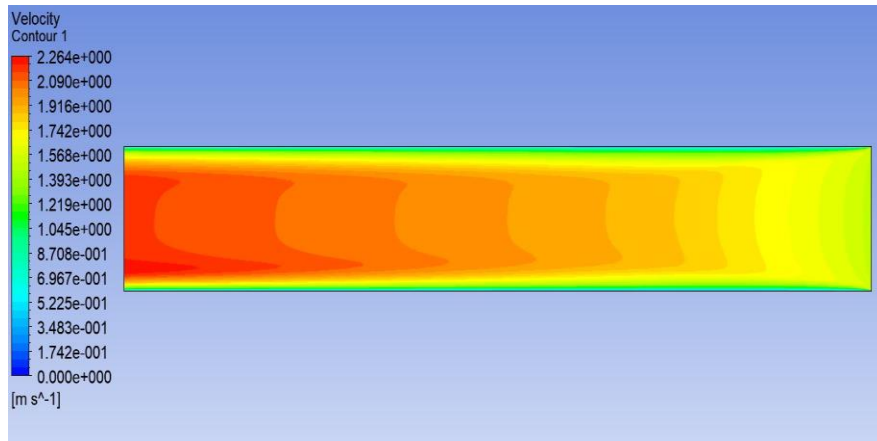

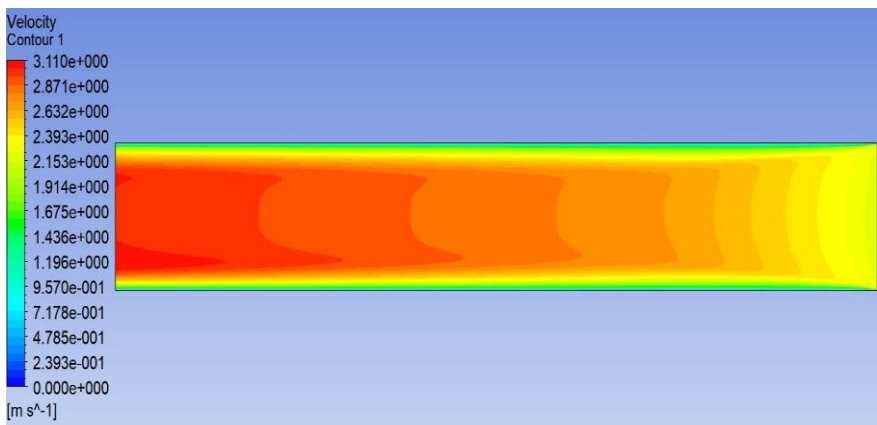*Figure 10 velocity distribution along y-z plane at P=7600Kpa, m=500kg/hr.m^2, T$_{in}$=307*

Figure 11 velocity distribution along y-z plane at P=8170Kpa, m=500kg/hr.m2, Tin=323

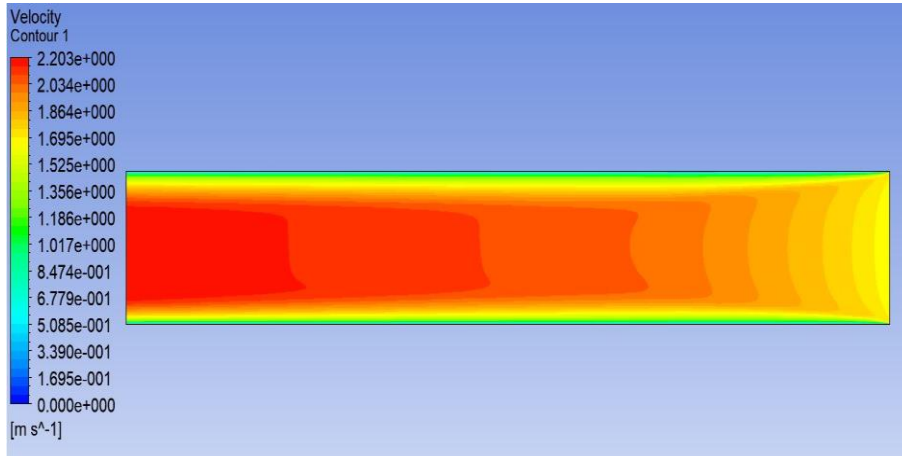*Figure 12 velocity distribution along a y-z plane at P=8170Kpa, m=1000kg/hr.m2, Tin=307*

To validate simulations, results are compared with experimental results. Six different turbulent models available in fluent are used for simulations and found that k-e, realizable with standard wall function has most close results to experiments. In further discussion results using this model will be discussed. Figure 13 shows a comparison of simulation results with experimental results. This is a case for inlet pressure of 8170 KPa and mass flux of 500 Kg/hr-m2. It shows that simulation results follow the trend observed in experimental results but heat transfer coefficient value, obtained from simulations, is very low as compared to experimental results. This offset of results may occur due to many reasons which are explained below.

First, in experimental setup total microchannel size is 50mm out of which 30mm is entry length. This length is provided to for flow to become fully developed. Only 20mm section of total 50mm length is heated. Due to computational power limitations, it was not possible to model whole 50mm length of the channel. So, how boundary layer development may affect the heat transfer in the system is completely unknown but it does contribute towards enhanced heat transfer.
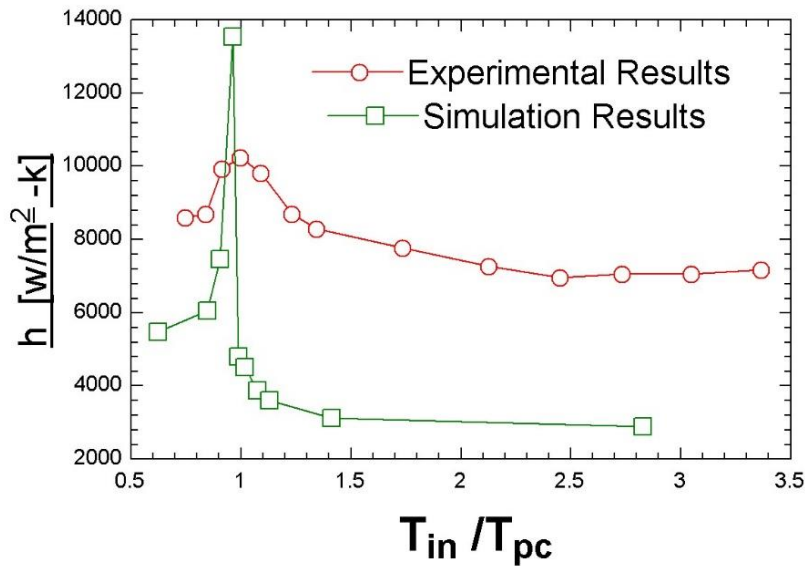
Figure 13 Comparison of simulation results with experimental results

Secondly, Figure 7 shows the schematic diagram of the test section. Although the length of the heated section is only 20mm there is no insulation between heated length and developing flow length. Heat will be conducted in solid part of the test section and fluid will gain heat in the developing region too. But for heat transfer coefficient calculations, effective heat transfer area accounts for the heated region only. This may be another reason for the difference between simulation and experimental results.

Research on microchannels do not have a long history and some research papers suggest that in actual boundary layer formation and flow is different in microchannels as compared to large size channel. Till now all the simulation research carried out on sCO$_2$ is in large-scale channels. No boundary layer file is available for supercritical CO$_2$. This is research area which needs attention to develop boundary layer files for supercritical flows in the microchannel and insert that file in the ANSYS Fluent to make simulations more realistic.

Finally, the literature shows that available fluid property models have 20% - 30% error from experimental data in the near-critical region. These are the few reasons which explain the difference between experimental and simulation results but further

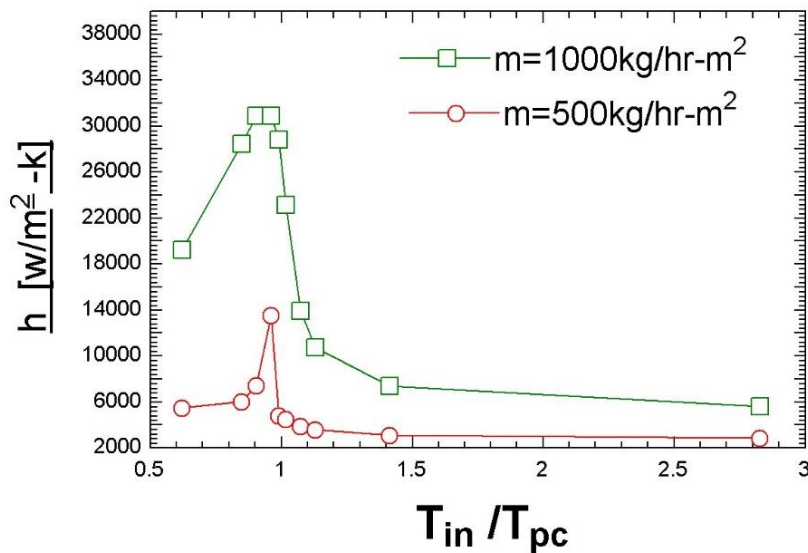research is needed to inspect and verify the effect boundry layer development on heat transfer.

Figure 14 Effect of mass flux on heat transfer coefficient

Figure 14 shows the effect of mass flow rate on heat transfer coefficient. Two different mass fluxes were modeled i.e. 500 kg/hr-m2 and 1000 kg/hr-m2. Inlet pressure and heat flux for this case were 8170 KPa and 20 W/cm2 respectively. Heat transfer coefficient peaks are obvious from Figure 14. These peaks occur near the Pseudocritical point of CO2. Beyond a pseudocritical point, heat transfer behavior is almost linear. It is also observed that heat transfer coefficient is higher for higher mass flow rate. At high mass flux, Reynolds number is increasing which indicate that turbulence of fluid is high. High turbulence causes heat transfer coefficient to increase significantly. Although the mass flow rate is doubled heat transfer coefficient increases more than double.

Figure 15 shows how heat flux affects heat transfer coefficient. The mass flow rate was set to 1000 kg/hr-m2. By increasing heat flux, heat transfer coefficient decreases. And finally, Figure 16 shows how heat transfer coefficient varies by changing inlet pressure of the fluid. Mass flow for this case was 500kg/hr-m^2. At

lower inlet pressures, heat transfer coefficient is lower as compared to that of higher inlet pressures. In all cases, heat transfer peaks are observed at the pseudocritical point of the CO_2 for that specific pressure.
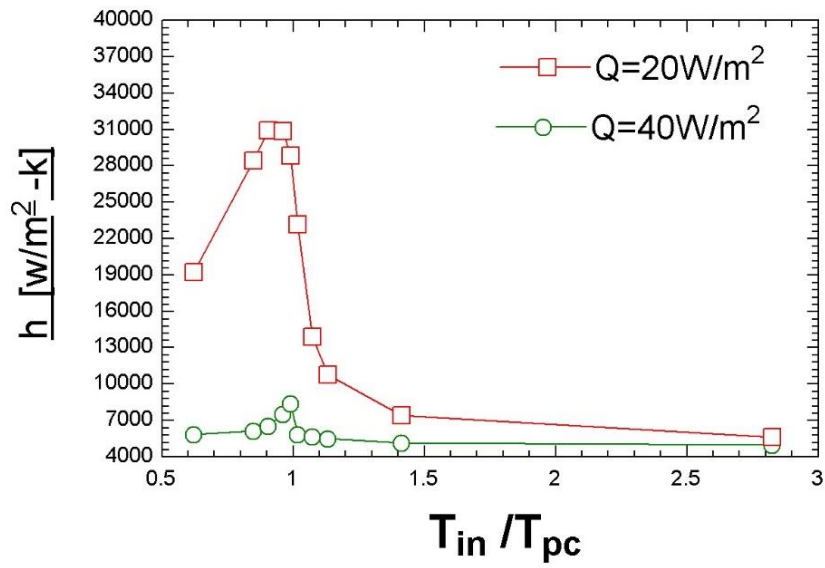

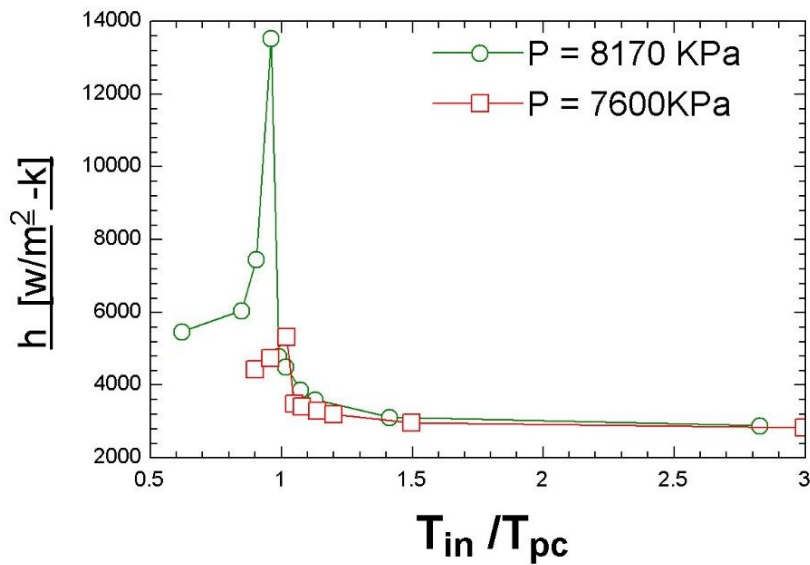*Figure 15 Effect of heat flux on heat transfer coefficient*

Figure 16 Effect of inlet pressure on heat transfer coefficient

5.2 Pressure Drop

Figure 17 shows how pressure drop varies with temperature at different inlet conditions. Pressure drop shown in this graph is a total pressure drop across the test sections. Pressure drop is measured for three different mass flow rates at different inlet temperatures while keeping inlet pressure constant. Then inlet pressure is varied for a mass flow rate of 10 kg/hr. As mentioned in Table 4, all pressure conditions are close to critical pressure to observe effects in the near-critical region. Also, temperature varies from 20°C to 50°C to observe pressure on both sides of the critical point. Pressure drop increases with increasing temperature. As we move towards higher temperature, Critical fluid properties changes in such a way that it shifts from liquid-like to gas like. The viscosity of gases increases at higher temperatures due to increased collisions of molecules. Higher viscosity leads to higher pressure drop.

Another effect is obvious from Figure 17 that slope of the curve is high at 30°C to 40°C. This is due to large properties variation which is shown in Figure 2. Before and after this region, the pressure drop has a very low slope.

Pressure drop increases significantly at higher mass flow rates. Because higher mass flow rate causes the flow to be more turbulent. Also, for two same mass flow rates pressure drop is higher for lower reduced pressure. Because it is closer to the critical region.

Figure 18 shows analytically calculated pressure drop variation with temperature and mass flow rate. Four different correlations, which are mentioned in the experimental setup, are used for pressure drop in microchannels. All these correlations are widely used for pressure drop in large channels but are not tested for microscale devices. Minor losses are calculated from available formulae in literature. It was found that Churchill and white correlations give identical results while fang and Blasius correlation have same results. So results from two correlations are plotted below. Black lines are results from Churchill correlations while blue lines are from Fang et al. Figure 18 shows that predicted pressure drop from Churchill correlation is higher than that of Fang et al. But both of these correlations follow the same trend as observed in experimental results.
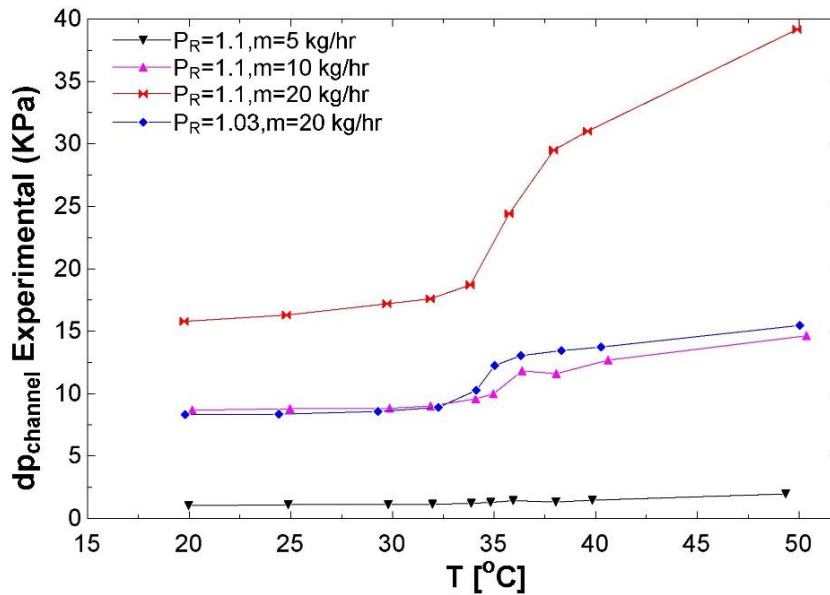

Figure 17 Effect of temperature on pressure drop for different inlet conditions
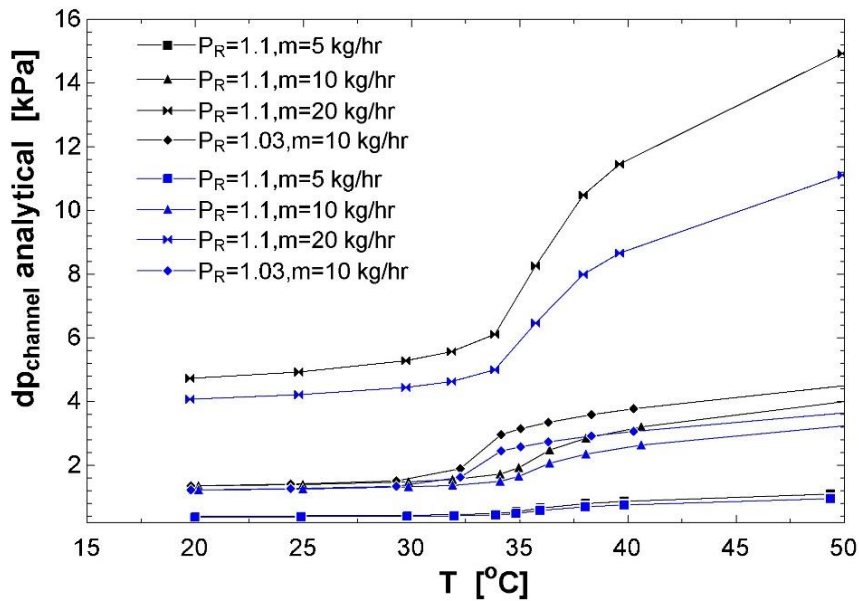
Figure 18 Effect of Temperature on theoretical pressure drop. Black lines represent pressure drop calculated from Churchill correlation while blue lines are pressure drop from Fang et al.

Figure 19 shows a comparison of experimental results and analytical results calculated from Churchill correlations on a log scale. Similarly, Figure 20 shows a comparison of experimental results with results from Fang et al. correlation. None of these correlations accurately predict pressure drop for microchannels. All these correlations are developed for large-scale channels. They are widely used in industries for pressure drop calculations and successfully calculate pressure drop. But in case of microchannel, the situation is much different. Also, all these correlations do not account for a large amount of property calculations which occurs in case of supercritical fluids. Another reason for this Difference is that flow in the microchannel is not fully developed but there is some entry length for fluid to become fully developed. All these correlations are developed or fully developed flow and are not suitable for developing a flow. In an industrial application or large test sections, this difference will be very small as compared to the overall pressure drop of the system. But in our case channel length is just 50mm. out of which entry length is 30mm. So pressure drop due to developing flow may be significant. Finally, inability to calculate minor loos accurately in test sections. No suitable formulae were found for given setup and small system to calculate minor losses. This inability

to calculate minor loss may also be the cause of some offset between experimental and analytical pressure drop. These are some reasons which can explain the difference between experimental and analytical results.
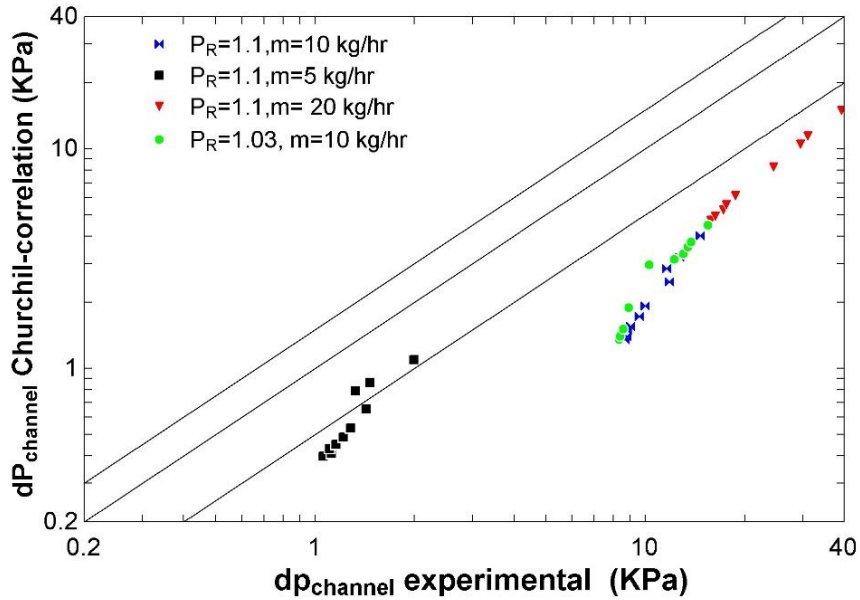

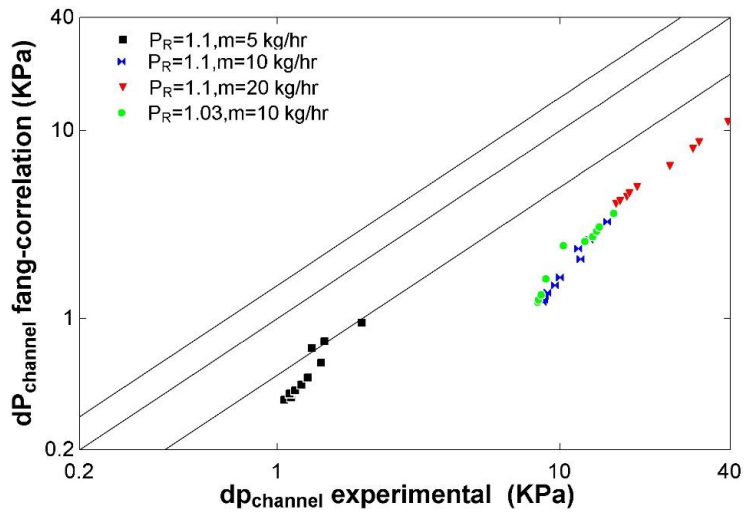*Figure 19 Pressure drop from Churchill correlation vs experimental pressure drop*

Figure 20 Pressure drop from Fang correlation vs experimental pressure drop

5.2.1 Uncertainty Analysis

For any experimental research, uncertainty analysis tells us about the reliability of the data. This technique is used to measure the uncertainty related to different quantities. In experiments, we used different instruments to measure physical quantities. Each instrument has an uncertainty associated with its results and is normally provided in equipment's data in the form of a percentage of measured value or full-scale reading. This uncertainty is known as design uncertainty. In most experiments, we use further calculation from measured quantities to get our required quantities are results. Uncertainty in measured values is than propagate to calculated quantities and is known as calculated uncertainty.

Independent quantities of pressure drop experiments are inlet pressure, mass flow rate and inlet temperature and pressure drop is the dependent variable. The pressure drop is measured experimentally using differential pressure transducer. Data points were taken for a minimum of 20 minutes after achieving steady state conditions at a frequency of 1Hz. During these 20 minutes, recorded data has slight variations within the uncertainty of the instrument. Following equations were used to calculate uncertainty.

$$\bar{x} = \frac{\sum_{i-1}^{N} Y_i}{N}$$

$$s = \sqrt{\frac{1}{N-1} \sum_{i=1}^{N} (Y_i - \bar{x})^2}$$

$$U_{Exp} = \pm \frac{t_{v,CI} \cdot s}{\sqrt{N}}$$

The dual-tailed Student t-distribution statistic is used here for the function of N - 1 degrees of freedom (v) and a confidence interval (CI) of 95% and valve of $t_{v,CI}$ is 1.69.

Instrument's design uncertainties are given in

Table 5 Instrumental uncertainty

Sr.No	Parameter	Uncertainty
1	Inlet Pressure	$\pm$ 6 Psi
2	Inlet Temperature	$\pm$ 0.25^{o}C
3	Pressure Drop	$\pm$ 0.25% of Full scale

So total uncertainty can be calculated by

$$U = \sqrt{\left(U_{Exp}\right)^2 + (U_{Des})^2}$$
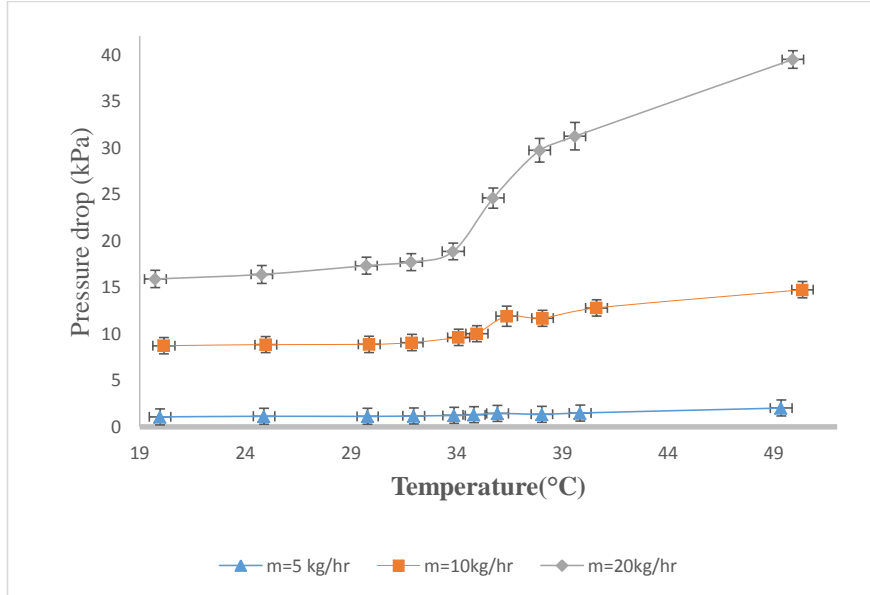

Figure 21 Uncertalinity in the experimental reuslts

6 Conclusion

From this research following results can be concluded.

1. Although simulation results follow the trends observed in experiments but do not match quantitatively.
2. Heat transfer coefficient has a peak value at the pseudocritical point and has almost varied linearly before and after the pseudocritical point. Heat transfer coefficient has increasing trend before the critical point and decreasing trend after the pseudocritical point.
3. Heat transfer coefficient increases at higher mass flux.
4. Heat transfer coefficient reduces at higher heat flux and lower reduced pressure.
5. Pressure drop increases with increasing temperature at a fixed mass flux and inlet pressure. The slope of the curve is high in near critical region between 30°C and 40°C and curve become almost flat before and after near-critical region.
6. Pressure drop Correlations follows the pattern of experimental results but very underpredict the value of pressure drop. Which shows that available correlations are unable to predict accurately pressure drop in microchannels and there is need to develop new correlations.

7 References

[1]   O. Behar, A. Khellaf, and K. Mohammedi, "A review of studies on central receiver solar thermal power plants," *Renew. Sustain. Energy Rev.*, vol. 23, pp. 12–39, 2013.

[2]   "Green Pro." [Online]. Available: http://www.genproenergy.com/learn/about-the-technology/solar-energy/solar-energy-facts-figures.html. [Accessed: 21-Aug-2017].

[3]   M. H. Sahir and A. H. Qureshi, "Assessment of new and renewable energy resources potential and identification of barriers to their significant utilization in Pakistan," *Renew. Sustain. Energy Rev.*, vol. 12, no. 1, pp. 290–298, 2008.

[4]   K. Vignarooban, X. Xu, A. Arvay, K. Hsu, and A. M. Kannan, "Heat transfer fluids for concentrating solar power systems - A review," *Appl. Energy*, vol. 146, pp. 383–396, 2015.

[5]   Y. Ahn *et al.*, "Review of supercritical CO2 power cycle technology and current status of research and development," *Nucl. Eng. Technol.*, vol. 47, no. 6, pp. 647–661, 2015.

[6]   H. A. Mohammed, G. Bhaskaran, N. H. Shuaib, and R. Saidur, "Heat transfer and fluid flow characteristics in microchannels heat exchanger using nanofluids: A review," *Renew. Sustain. Energy Rev.*, vol. 15, no. 3, pp. 1502–1512, 2011.

[7]   Y. Han, Y. Liu, M. Li, and J. Huang, "A review of development of micro-channel heat exchanger applied in air-conditioning system," *Energy Procedia*, vol. 14, pp. 148–153, 2012.

[8]   I. L. Pioro and R. B. Duffey, "Experimental heat transfer in supercritical water flowing inside channels (survey)," *Nucl. Eng. Des.*, vol. 235, no. 22, pp. 2407–2430, 2005.

[9]   J. D. Jackson, "Fluid flow and convective heat transfer to fluids at supercritical pressure," *Nucl. Eng. Des.*, vol. 264, pp. 24–40, 2013.

[10]   S. M. Liao and T. S. Zhao, "Measurements of Heat Transfer Coefficients From Supercritical Carbon Dioxide Flowing in Horizontal Mini/Micro Channels," *J. Heat Transfer*, vol. 124, no. 3, p. 413, 2002.

[11]   L. Chen, Y. M. Chen, M. H. Sun, and X. R. Zhang, "Investigation of trans-critical CO2 horizontal mini-channel flow with multi-peak heat transfer behaviors," *Ann. Nucl. Energy*, vol. 75, pp. 559–569, 2015.

[12]   L. Chen, X. R. Zhang, J. Okajima, and S. Maruyama, "Numerical investigation of near-critical fluid convective flow mixing in microchannels," *Chem. Eng. Sci.*, vol. 97, pp. 67–80, 2013.

[13]   S. Koshizuka, "Numerical analysis of deterioration phenomena in heat transfer to supercritical water," *Int. J. Heat Mass Transf.*, vol. 38, no. 16, pp. 3077–3084, 1995.

[14]   S. H. Yoon, J. H. Kim, Y. W. Hwang, M. S. Kim, K. Min, and Y. Kim, "Heat transfer and pressure drop characteristics during the in-tube cooling process of carbon dioxide in the supercritical region," *Int. J. Refrig.*, vol. 26, no. 8, pp. 857–864, 2003.

[15]   M. Sharabi, W. Ambrosini, S. He, and J. D. Jackson, "Prediction of turbulent convective heat transfer to a fluid at supercritical pressure in square and triangular channels," *Ann. Nucl. Energy*, vol. 35, no. 6, pp. 993–1005, 2008.

[16]   S. Pandey, X. Chu, and E. Laurien, "Investigation of in-tube cooling of carbon dioxide at supercritical pressure by means of direct numerical simulation," *Int. J. Heat Mass Transf.*, vol. 114, pp. 944–957, 2017.

[17]   M. Xiang, J. Guo, X. Huai, and X. Cui, "Thermal analysis of supercritical pressure CO 2 in horizontal tubes under cooling condition," *J. Supercrit. Fluids*, vol. 130, no. January, pp. 389–398, 2017.

[18]   Z.-B. Liu, Y.-L. He, Y.-F. Yang, and J.-Y. Fei, "Experimental study on heat transfer and pressure drop of supercritical CO2 cooled in a large tube," *Appl. Therm. Eng.*, vol. 70, no. 1, pp. 307–315, 2014.

[19]   K. Tanimizu and R. Sadr, "Experimental investigation of buoyancy effects on convection heat transfer of supercritical CO2 flow in a horizontal tube," *Heat Mass Transf.*, 2015.

[20]   Kyle R. Zada, "Experimental Investigation of Supercritical Heat Transfer of Carbon Dioxide in Parallel Square Microchannels with a Single-Wall Constant Heat Flux Boundary Condition," Oregon State University, Oregon, 2017.

[21]   H. Kudela, "Hydraulic losses in pipes," *Chart*, no. 3, 2010.

[22]   Crane Co., "Flow Of Fluids Through Valve, Fittings and Pipe." p. 133, 1982.

[23]   T. Rostrup-nielsen, *Thermal Energy Systems*. 2010.

[24]   S. H. Yoon, J. H. Kim, Y. W. Hwang, M. S. Kim, K. Min, and Y. Kim, "Heat transfer and pressure drop characteristics during the in-tube cooling process of carbon dioxide in the supercritical region," *Int. J. Refrig.*, vol. 26, no. 8, pp. 857–864, 2003.

[25]   S. T. Jostein Pettersen, Rene Reiberer, "Heat Transfer and Pressure Drop for Flow of supercritical and subcritial CO2 in micro channel tubes," 2000.

[26]   X. Fang, Y. Xu, X. Su, and R. Shi, "Pressure drop and friction factor correlations of supercritical flow," *Nucl. Eng. Des.*, vol. 242, pp. 323–330, 2012.

[27]   L. Cheng, G. Ribatski, and J. R. Thome, "Analysis of supercritical CO2 cooling in macro- and micro-channels," *Int. J. Refrig.*, vol. 31, no. 8, pp. 1301–1316, 2008.

8 Appendices

Table 6 Simulation results for m=500kg/m^2-hr, P$_{in}$=8170 kPa, Q=20 W/cm^2

T$_{in}$	T$_{out, area avg.}$	T$_{out, mass avg.}$	T$_W$
295	302.68	300.98	332.17
300	305.63	305.42	312.50
303	308.1	306.35	341.92
305	309.71	307.63	345.26
307	308.95	308.81	325.24
308	312.34	309.90	350.71
309	314.14	311.26	354.34
311	319.88	315.98	364.42
313	324.37	320.03	371.00
323	341.054	335.482	391.65
373	398.054	392.61	450.013

Table 7 Simulation results for m=1000kg/m^2-hr, P$_{in}$=8170 kPa, Q=20 W/cm^2

T$_{in}$	T$_{out, area avg.}$	T$_{out, mass avg.}$	T$_W$
295	299.24	298.57	310.30
303	305.46	305.035	313.86
305	306.867	306.51	314.93
307	308.24	307.93	316.60
308	309.00	308.69	317.99
309	310.087	309.65	320.83
311	313.21	312.52	328.99
313	316.71	315.60	335.63
323	330.07	328.34	354.79
373	384.74	377.82	414.57

Table 8 Simulation results for m=1000kg/m^2-hr, P$_{in}$=8170 kPa, Q=40 W/cm^2

T$_{in}$	T$_{out, area avg.}$	T$_{out, mass avg.}$	T$_W$
295	304.35	300.74	358.74
303	311.49	306.55	375.84
305	313.05	308.04	378.80
307	314.50	309.61	380.57
308	315.33	310.52	381.02
309	316.56	311.85	381.19
311	321.87	316.57	386.56
313	326.12	320.54	391.58
323	341.9	-	409.1

373	398.77	39.60	465.09

Table 9 Simulation results for m=1000kg/m^2-hr, P$_{in}$=7600 kPa, Q=20 W/cm^2

T$_{in}$	T$_{out, area avg.}$	T$_{out, mass avg.}$	T$_W$
303	307	305.14	348.42
305	308.53	306.32	350.18
307	316.57	312.07	363.01
308	319.48	314.61	367.42
309	321.5	316.57	370.14
311	324.88	319.97	374.49
313	328.51	323.29	378.98
323	342.86	337.10	395.23
373	398.89	393.15	451.27